Supplementary Materials for

Direct integration of modular stretchable system for implantable bioelectronics

Yesol Kim[1,2⊥], Hoechang Chung[1,2⊥], Chanhui Park[1,2⊥], Seonghyeon Nam[1,2], Sung-Hyuk Sunwoo[1, 3*], and Dae-Hyeong Kim[1,2*]

[1]*Center for Nanoparticle Research, Institute for Basic Science (IBS), Seoul 08826, Republic of Korea.*

[2]*School of Chemical and Biological Engineering, Institute of Chemical Processes, Seoul National University, Seoul 08826, Republic of Korea.*

[3]*Department of Chemical Engineering, Inha University, 100 Inha-ro, Michuhol-gu, Incheon 22212, Republic of Korea.*

[⊥]These authors equally contributed to this work.

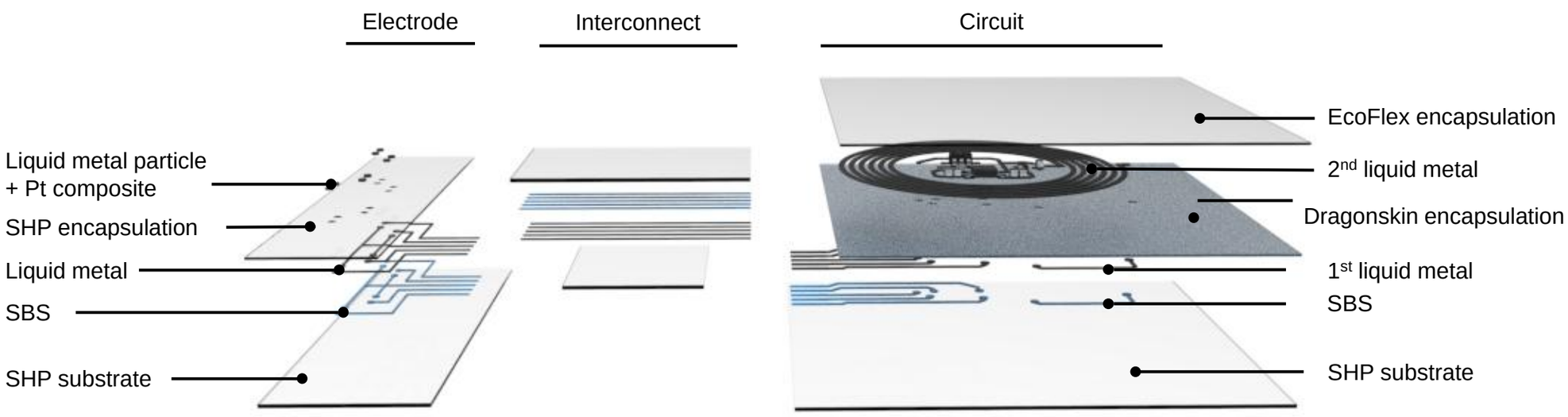
*To whom correspondences should be addressed.

The PDF file includes:

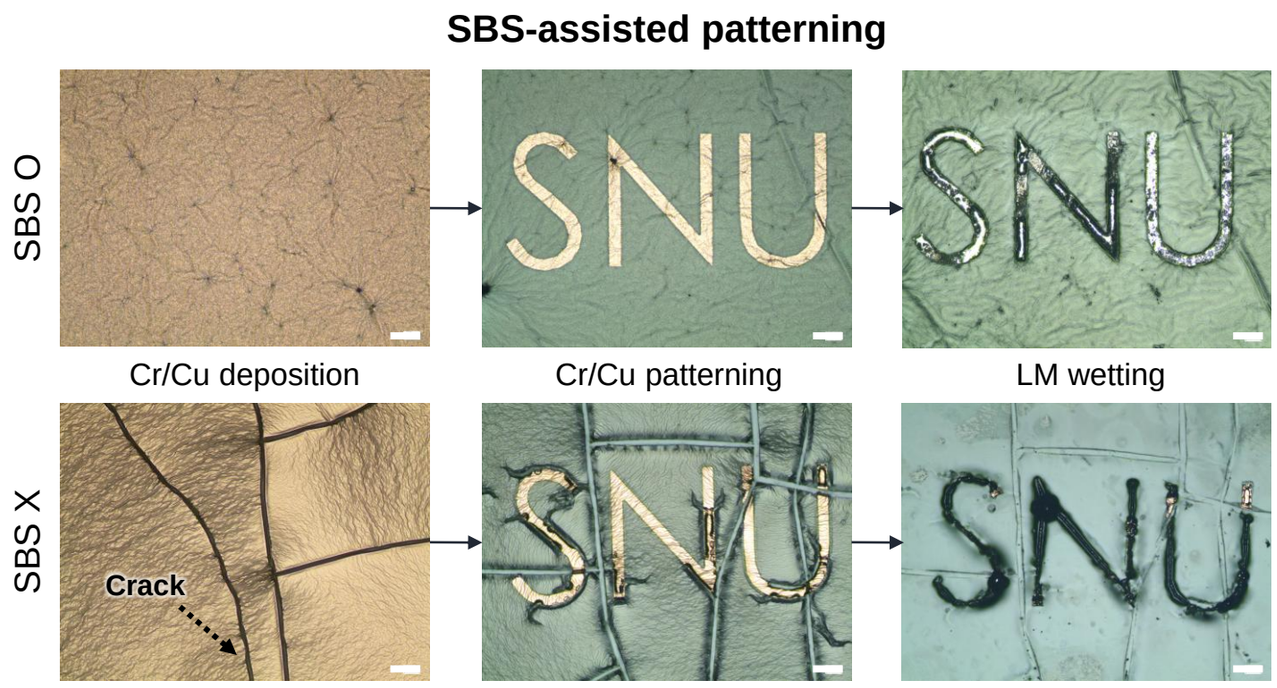
Figs. S1 to S23

Other supplementary Materials for this manuscript include:

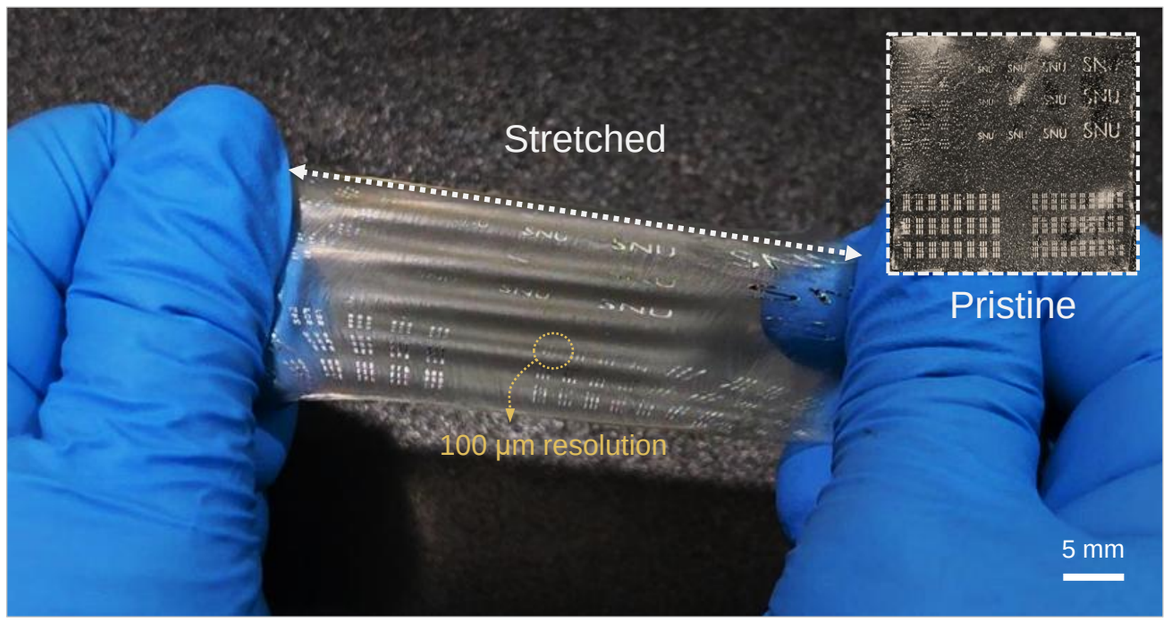
Supplementary Video S1



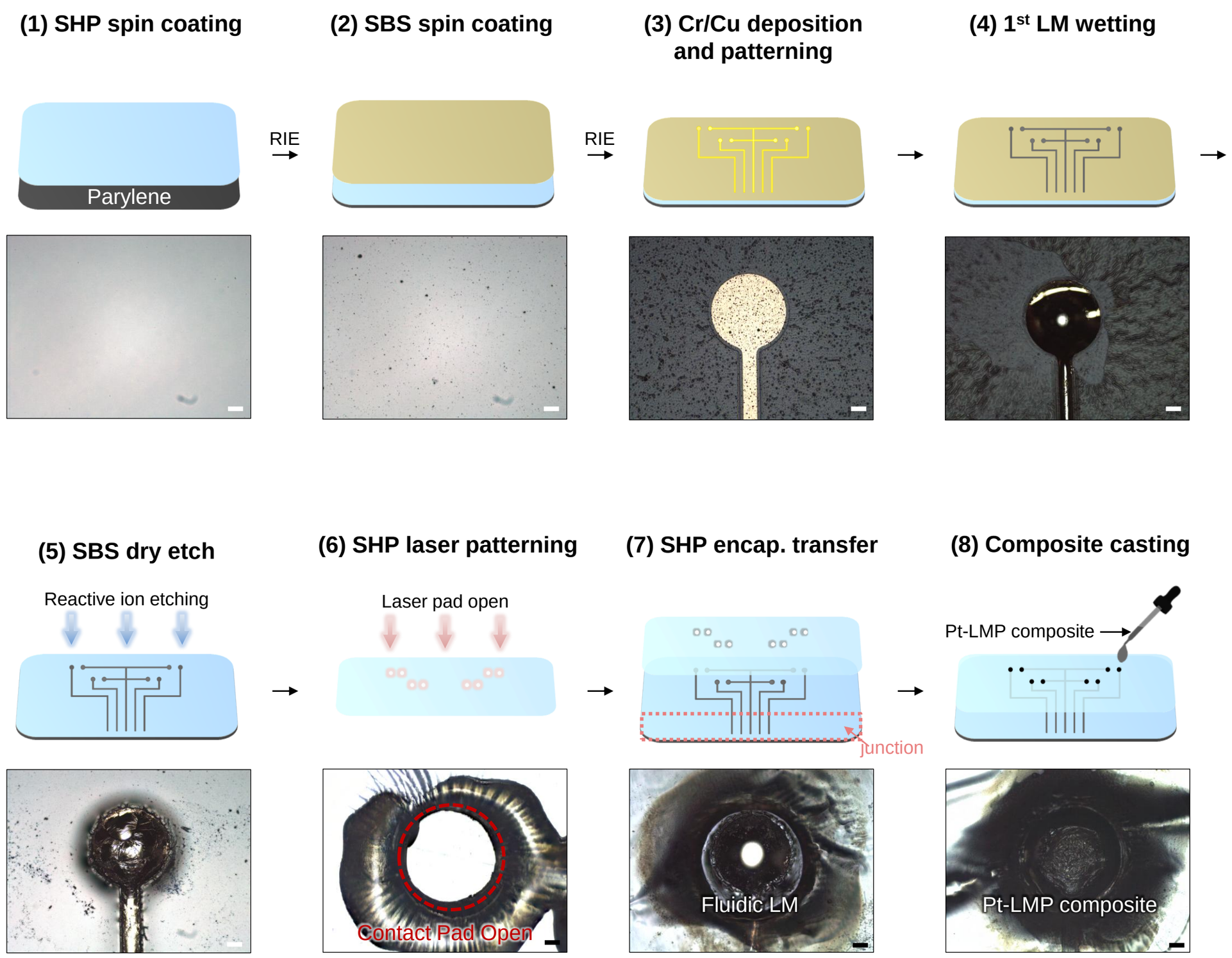
Supplementary Fig. 1. Layer architecture of the stretchable bioelectronic modules. Exploded schematics of the electrode, interconnect, and circuit modules showing the constituent SHP, SBS, liquid metal, encapsulation, and Pt-LMP composite layers.



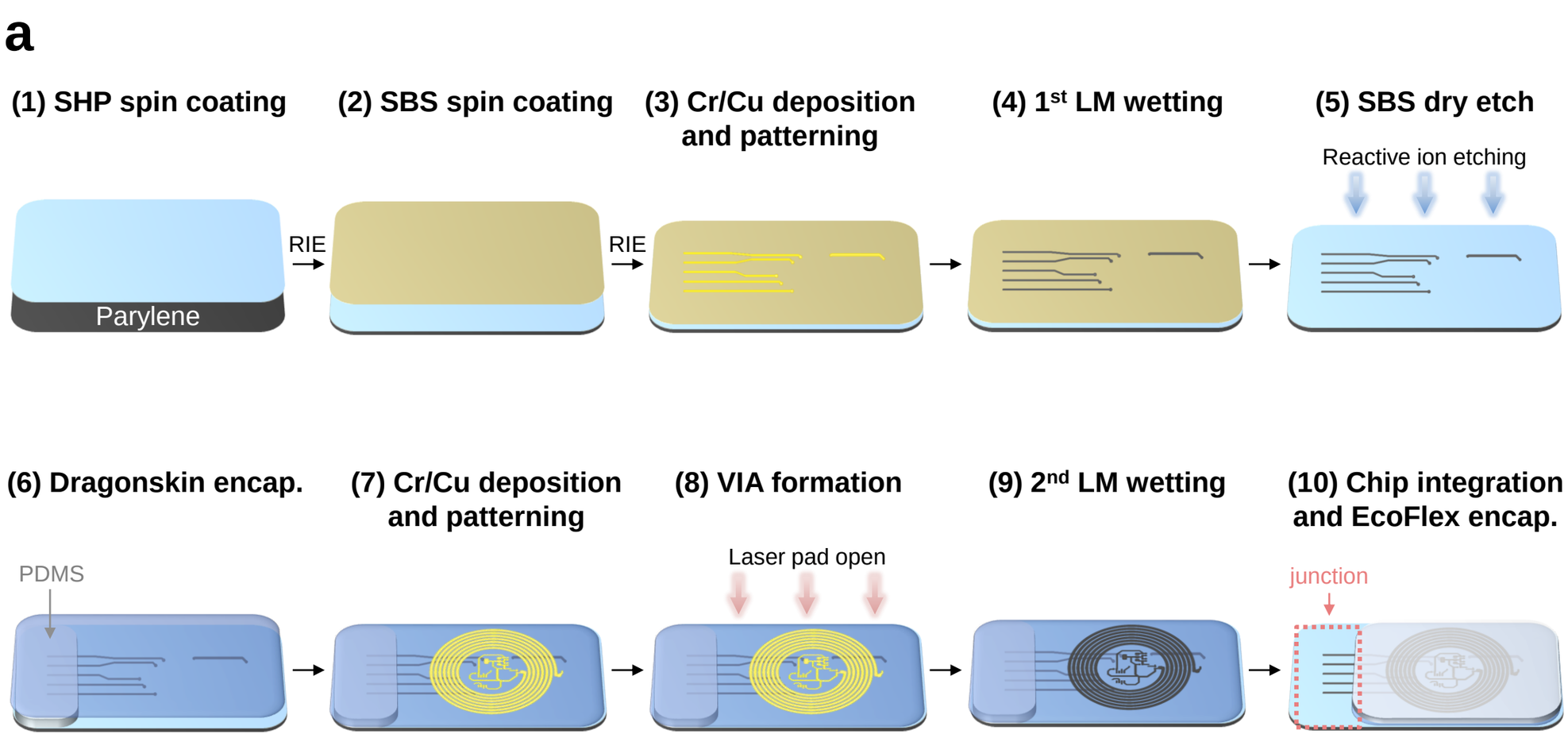
Supplementary Fig. 2. SBS-assisted photolithography on self-healing polymer substrates. Optical images of Cr/Cu patterning, photopatterning and subsequent liquid metal wetting on self-healing polymer substrates, with or without the SBS processing layer. Scale bar is 200 μm.



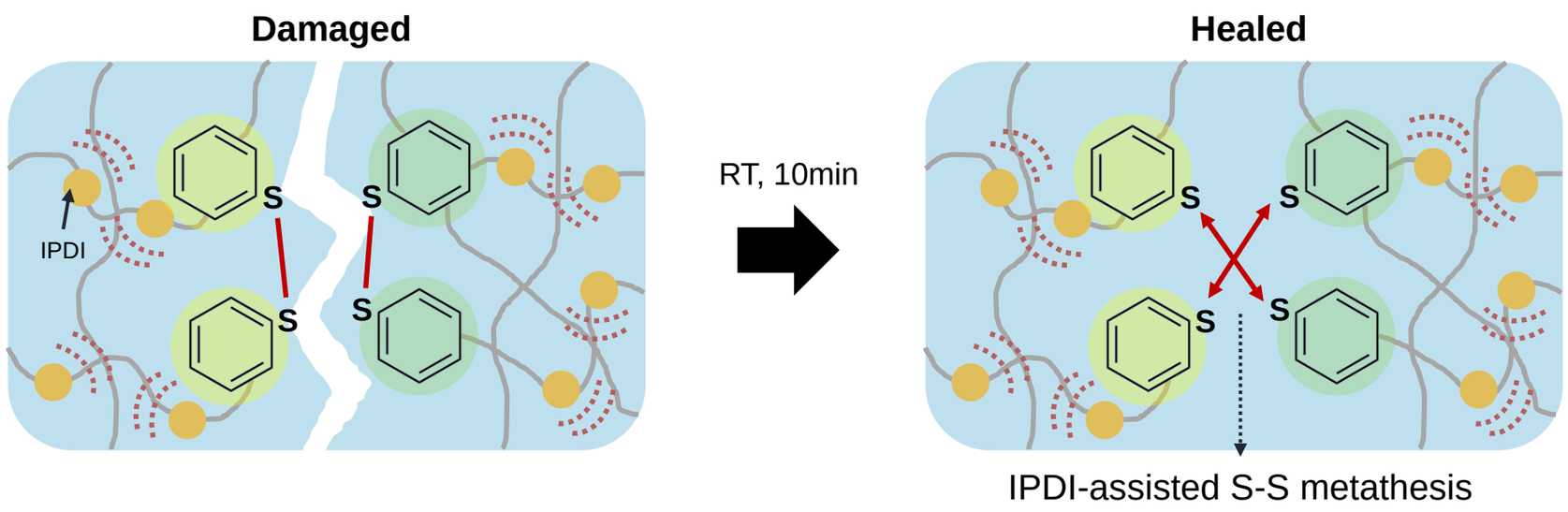
Supplementary Fig. 3. High-resolution liquid metal patterning on self-healing polymer substrates. Optical images of liquid metal patterns with a minimum feature size of 100 μm, showing reliable pattern integrity in both pristine and stretched states.



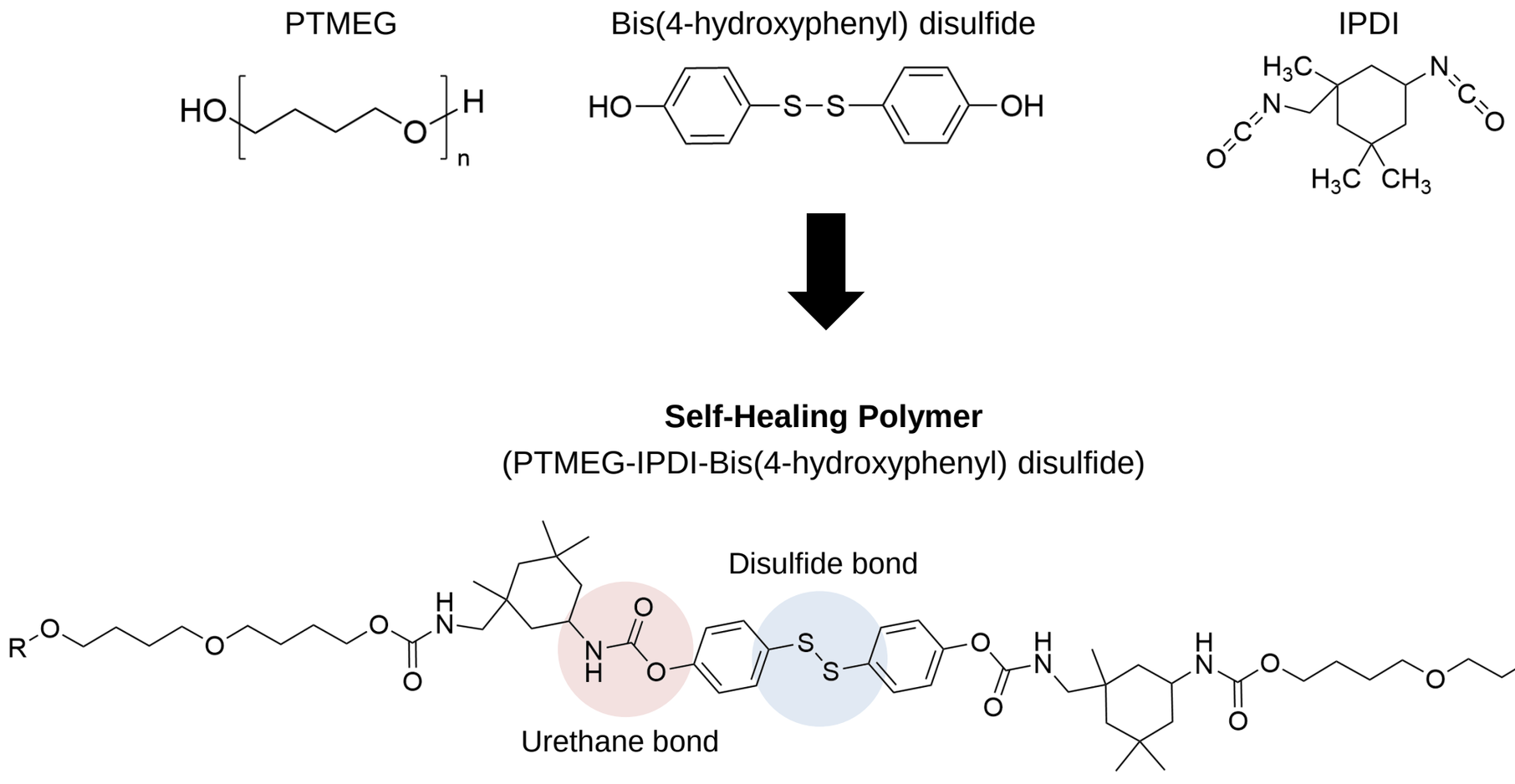
Supplementary Fig. 4. Fabrication process of the stretchable electrode module. Schematics (top) and optical microscope images (bottom) showing the sequential fabrication process of the electrode module. Scale bar is 200 μm.



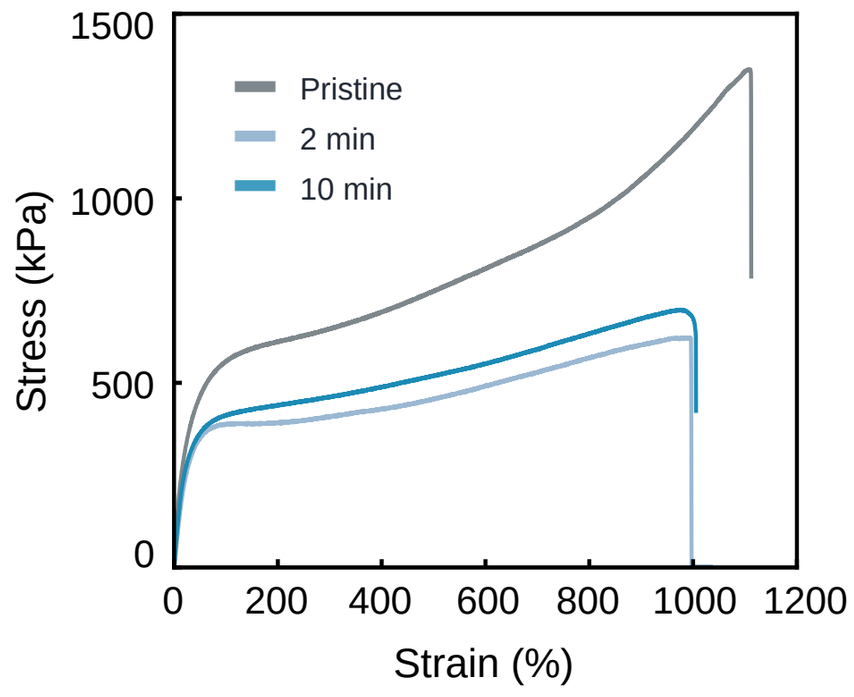
Supplementary Fig. 5. Fabrication process of the multi-layer stretchable circuit module. a, Schematics (top) and optical microscope images (bottom) showing the sequential fabrication process of the multi-layer circuit module. **b,** Optical images showing formation of the vertical interconnection access (VIA) between the first and second liquid metal layers. Scale bar is 200 μm. **c,** Cross-sectional schematic of the multi-layer architecture and the VIA structures.



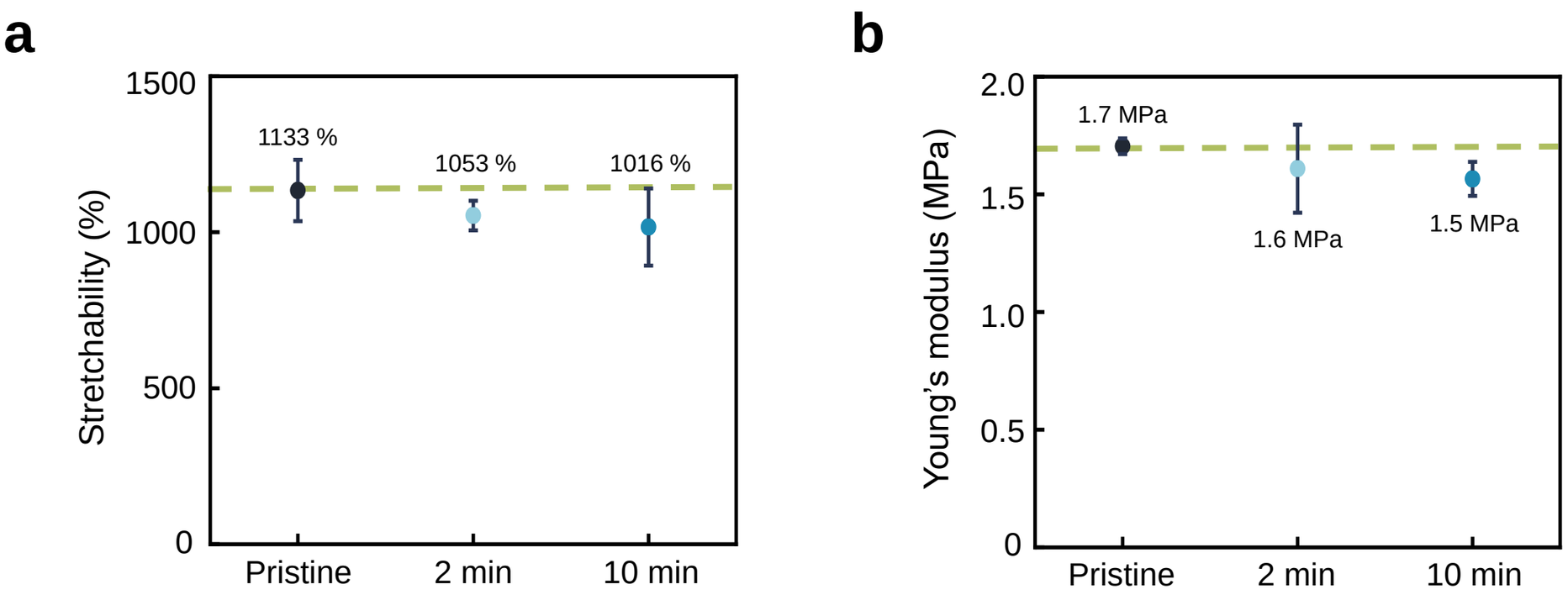
Supplementary Fig. 6. Schematic illustration of the disulfide-mediated self-healing mechanism. Schematic illustration of interfacial reconstruction through dynamic disulfide exchange after contacting damaged SHP surfaces at room temperature, 10 min conditions.



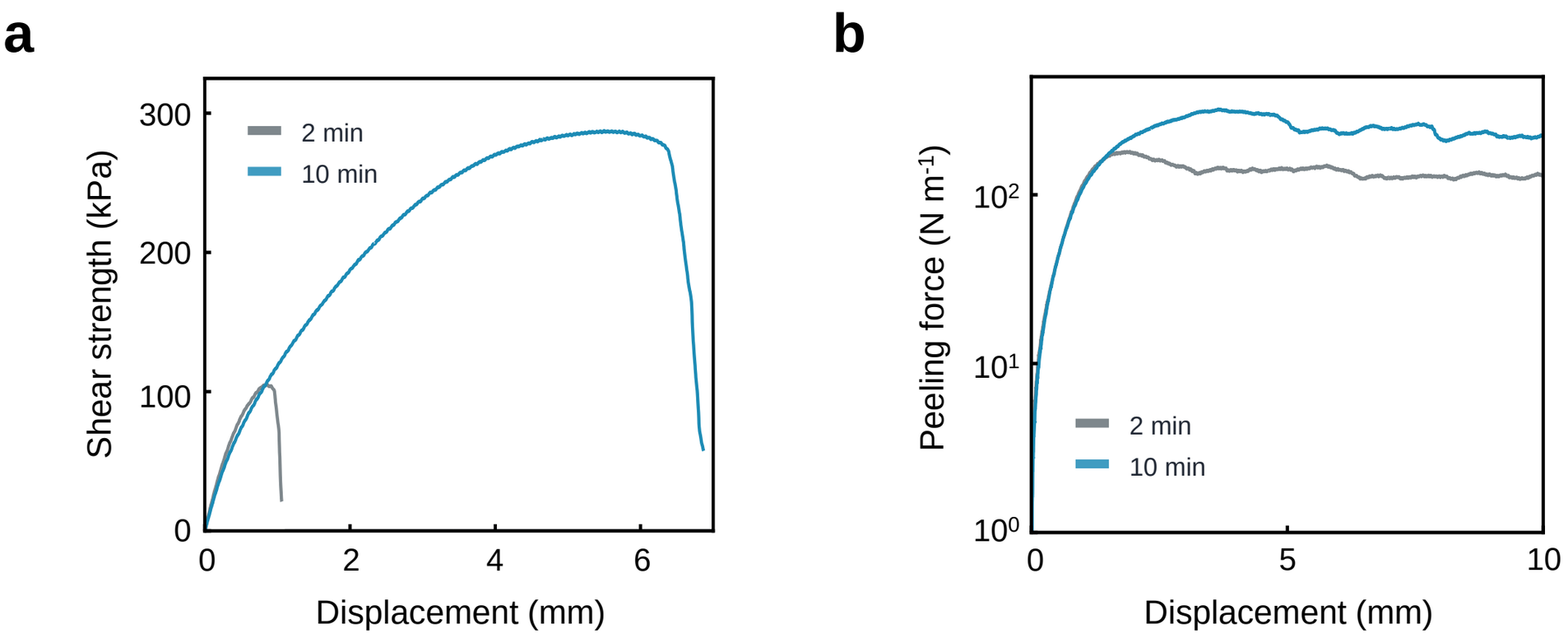
Supplementary Fig. 7. Molecular design and chemical structure of self-healing polymer. Chemical structure of the SHP synthesized from PTMEG, bis(4-hydroxyphenyl) disulfide and IPDI, incorporating urethane and dynamic disulfide bonds.



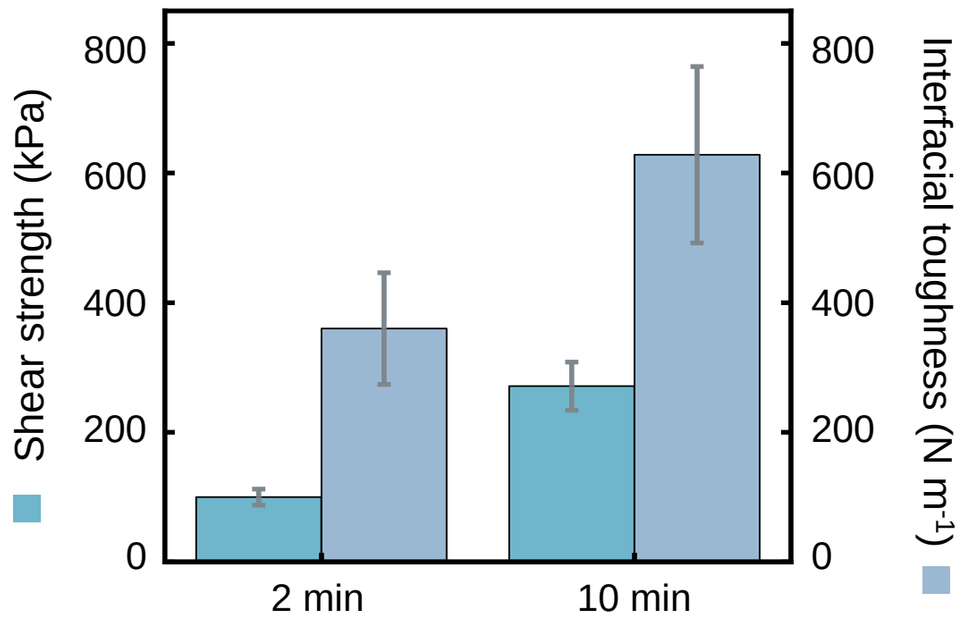
Supplementary Fig. 8. Mechanical recovery of self-healing polymer junctions. Stress–strain curves of pristine SHP and SHP junctions formed after 2 min and 10 min of contact at room temperature.



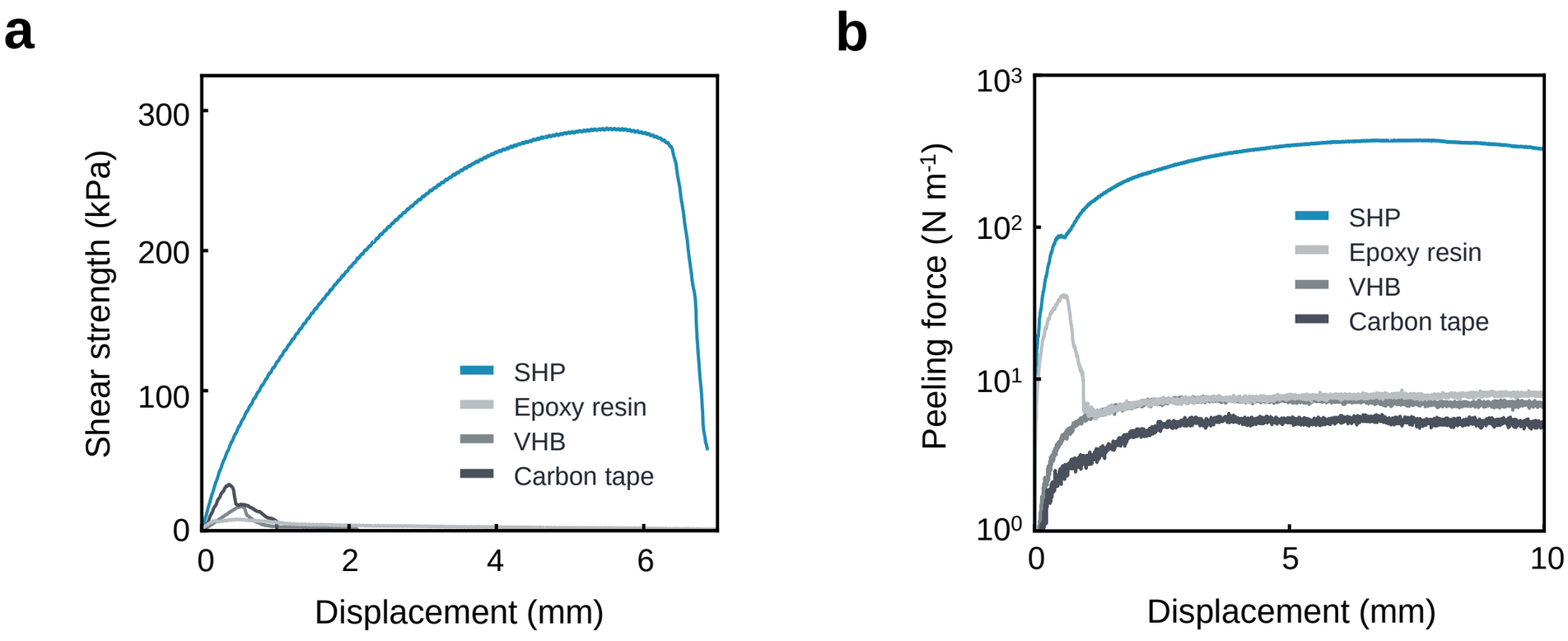
Supplementary Fig. 9. Stretchability and Young's modulus of self-healing polymer junctions. a, Stretchability and **b,** Young's modulus of pristine SHP and SHP junctions formed after 2 min and 10 min of contact at room temperature. Error bars are standard deviation from 3 samples.



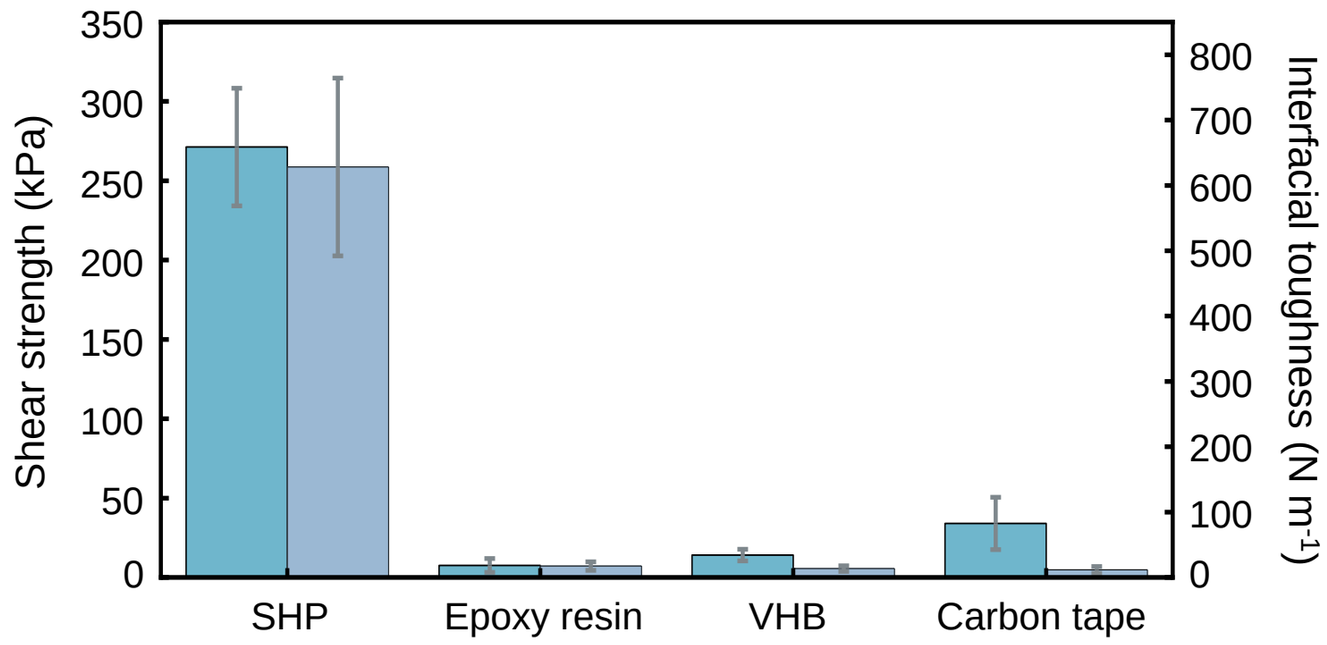
Supplementary Fig. 10. Time-dependent interfacial adhesion strength of self-healing polymer junctions. a, Representative lap-shear responses. **b,** Representative 180° peel responses of SHP junctions formed after 2 and 10 min of contact at room temperature.



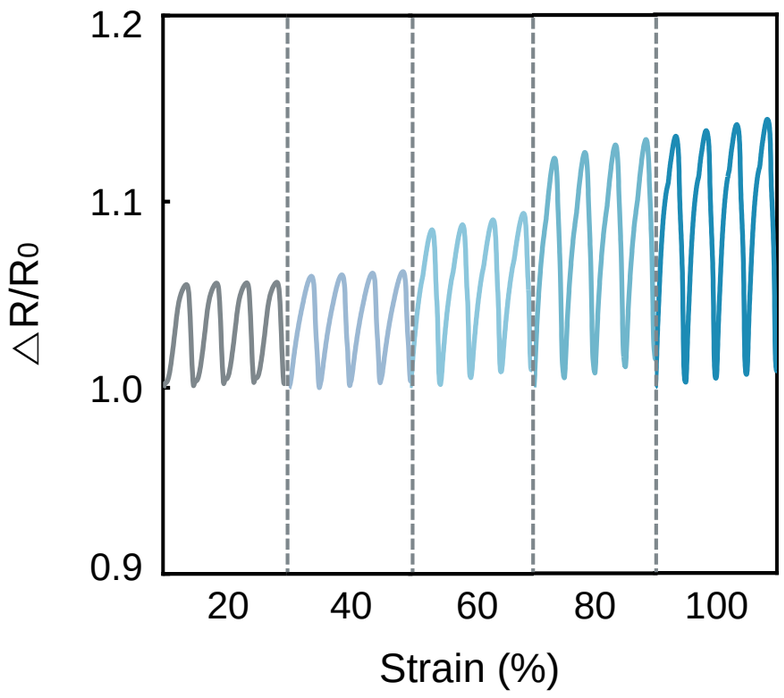
Supplementary Fig. 11. Time-dependent shear strength and interfacial toughness of self-healing polymer junctions. Quantified shear strength and interfacial toughness of SHP junctions after 2 min and 10 min of contact (overlapping area 10 mm width x 10 mm length). Error bars are standard deviation from 3 samples.



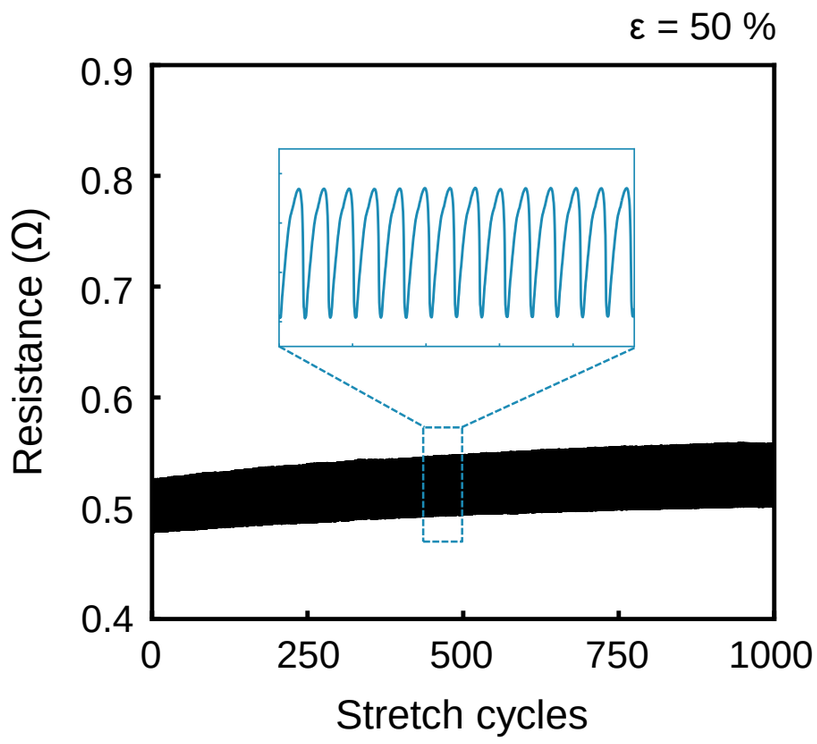
Supplementary Fig. 12. Comparison of adhesion responses of self-healing polymer and conventional bonding materials. a, Representative lap-shear responses. **b,** Representative 180° peel responses of SHP, epoxy resin, VHB and carbon tape.



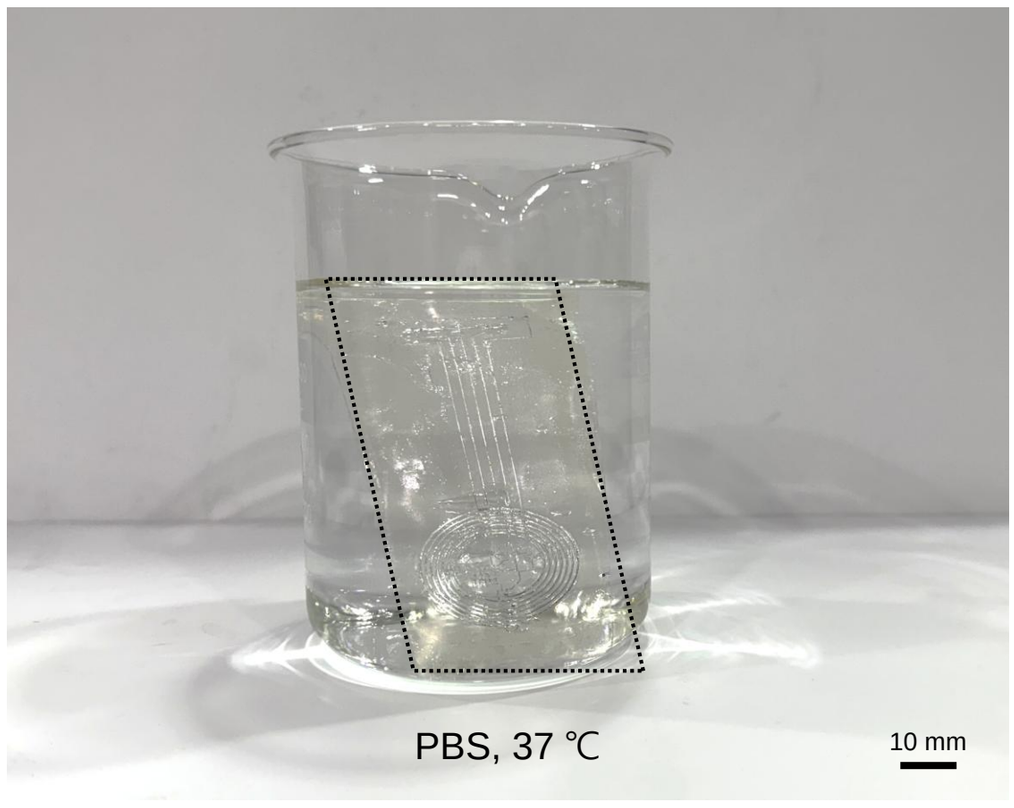
Supplementary Fig. 13. Comparison of interfacial adhesion strength of self-healing polymer and conventional bonding materials. Quantified shear strength and interfacial toughness of SHP junctions compared with conventional bonding materials; epoxy resin, VHB and carbon tape. Error bars are standard deviation from 3 samples.



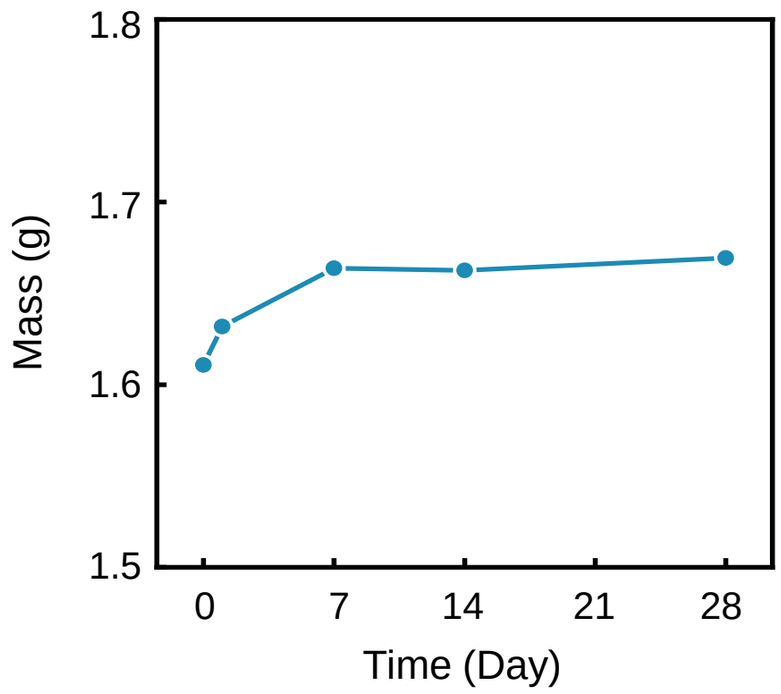
Supplementary Fig. 14. Strain-dependent electrical response of the stretchable interconnect module. Relative resistance change ($\Delta R/R_0$) of the interconnect during cyclic stretching at tensile strains of 20%, 40%, 60%, 80% and 100%.



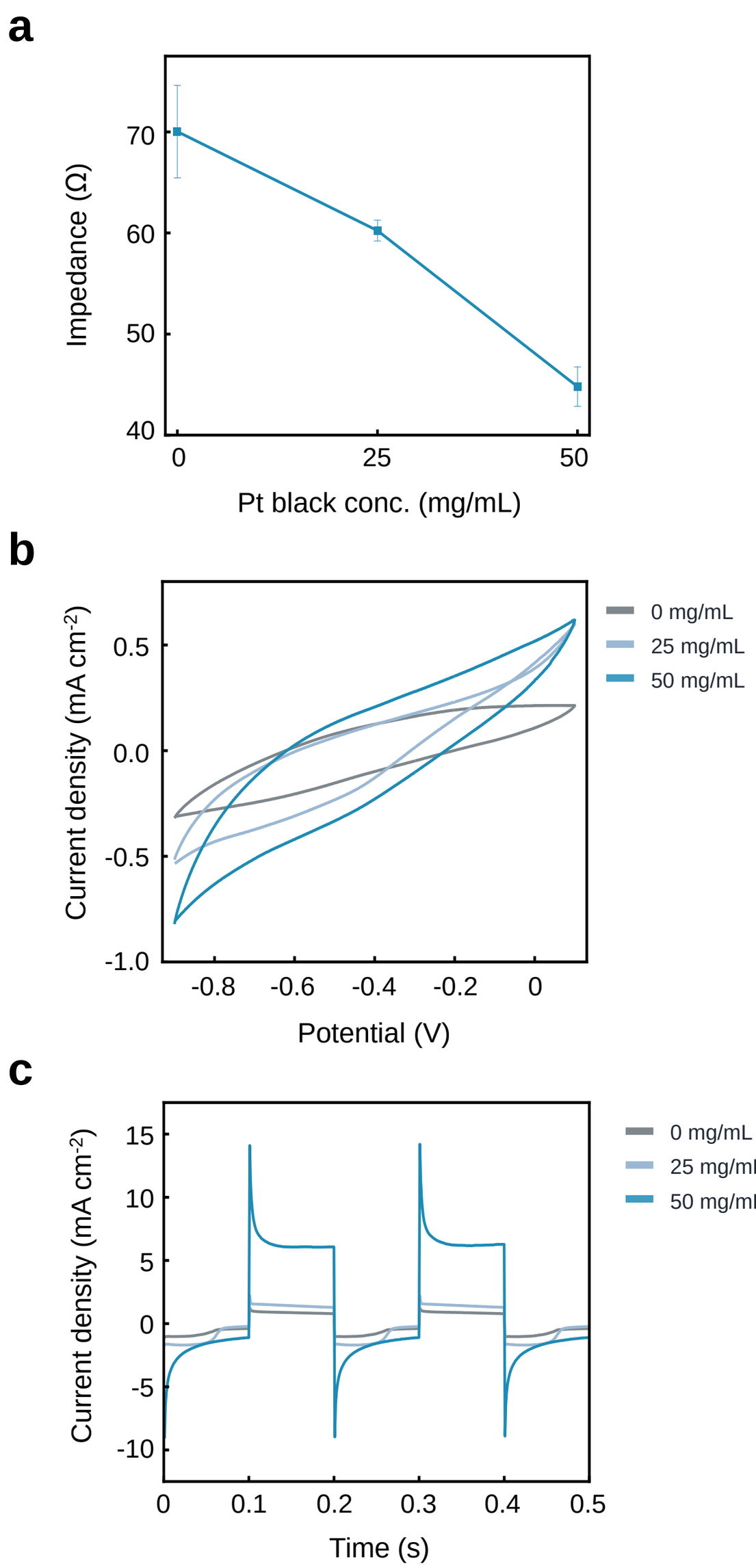
Supplementary Fig. 15. Cyclic electrical stability of the stretchable interconnect module. Resistance of the interconnect during 1,000 stretching cycles at 50% strain. Inset shows an enlarged segment of the cyclic response.



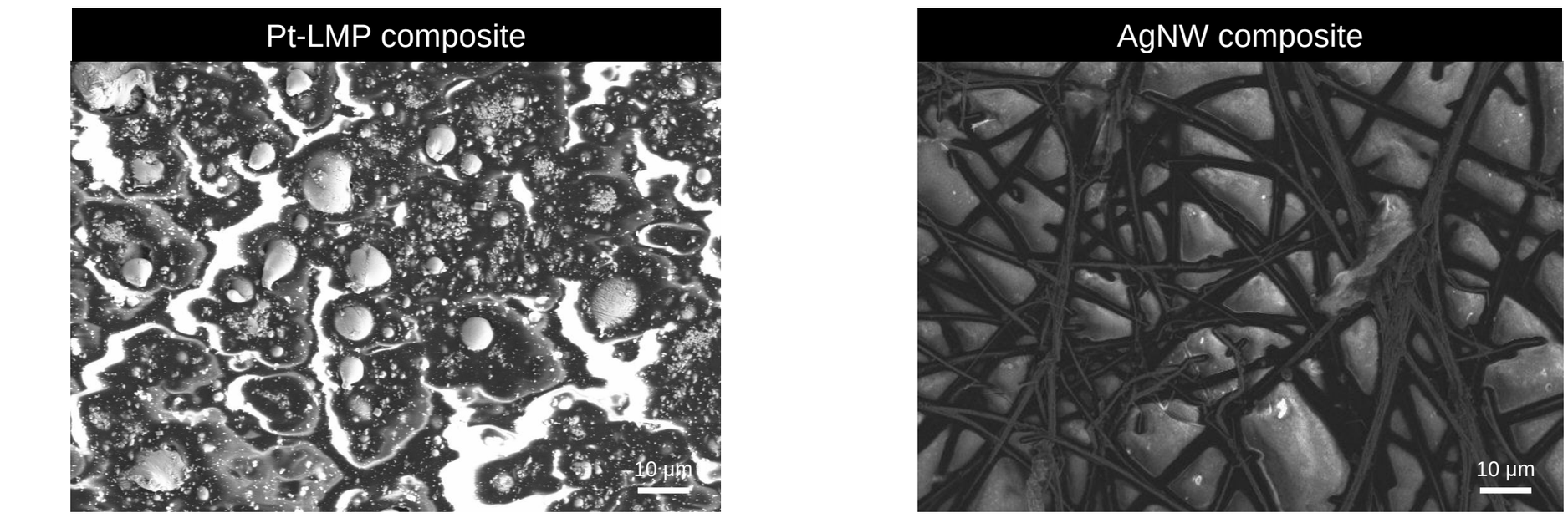
Supplementary Fig. 16. Experimental setup for long-term PBS immersion. Photograph of an integrated sample immersed in PBS at 37 °C for long-term stability evaluation.



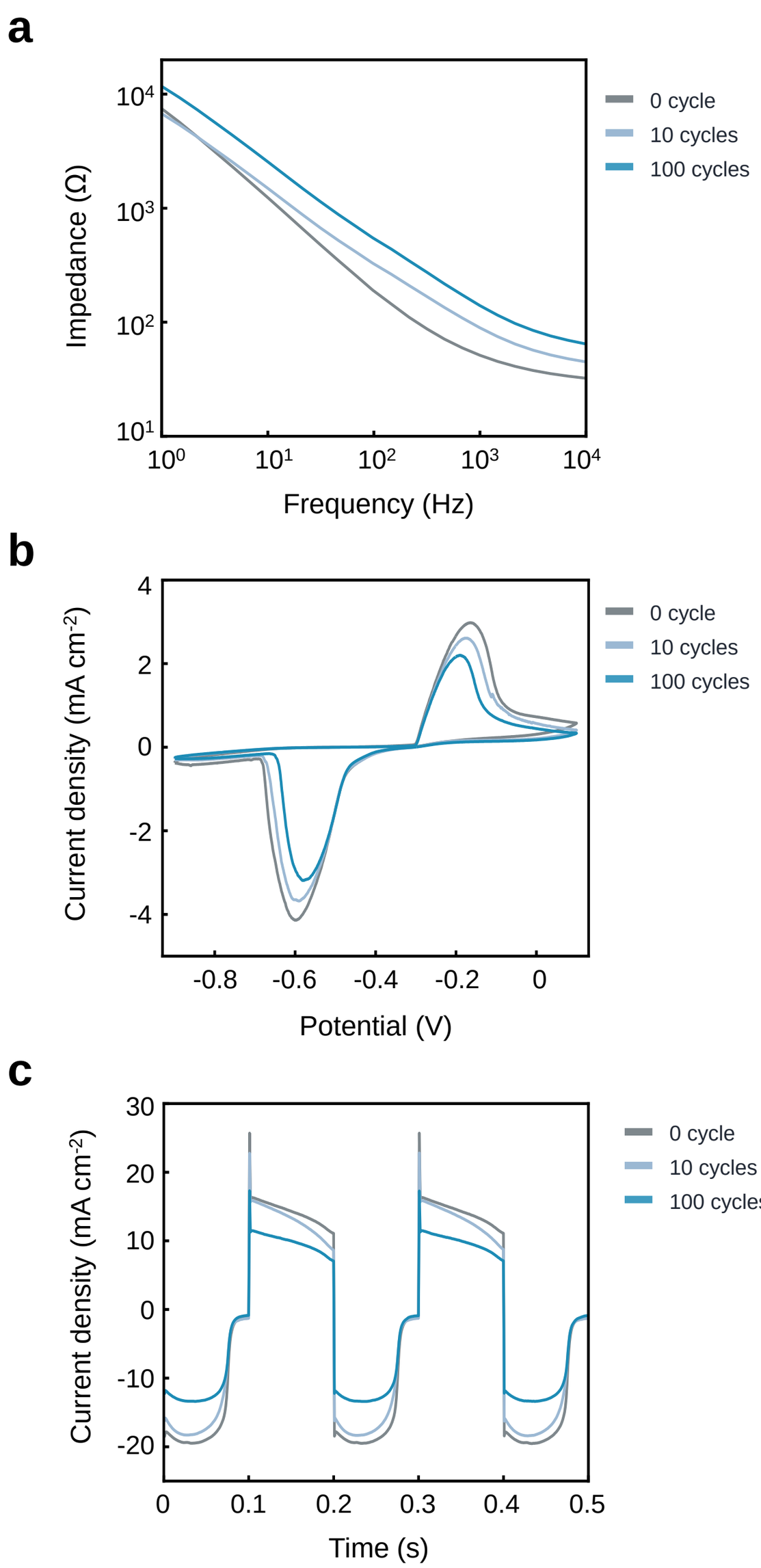
Supplementary Fig. 17. Mass stability of the self-healing polymer during long-term PBS immersion. Mass change of the integrated SHP sample immersed in PBS at 37 °C for 28 days.



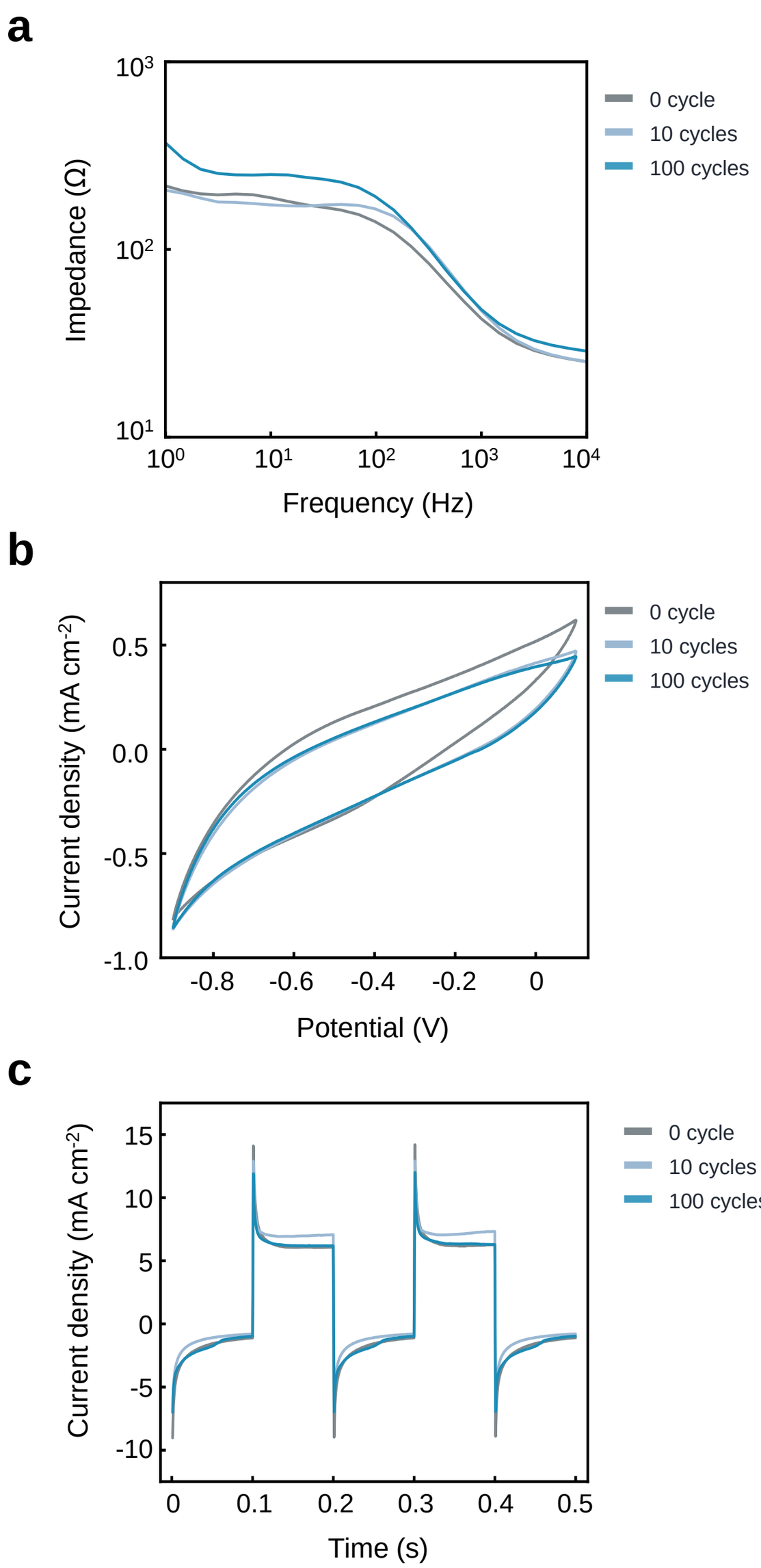
Supplementary Fig. 18. Effect of Pt black loading on the electrochemical characteristics of Pt-LMP electrodes. a, Impedance at 1 kHz. **b,** Cyclic voltammograms. **c,** Biphasic-pulse current responses of Pt-LMP electrodes with different Pt black concentrations (0, 25 and 50 mg/mL).



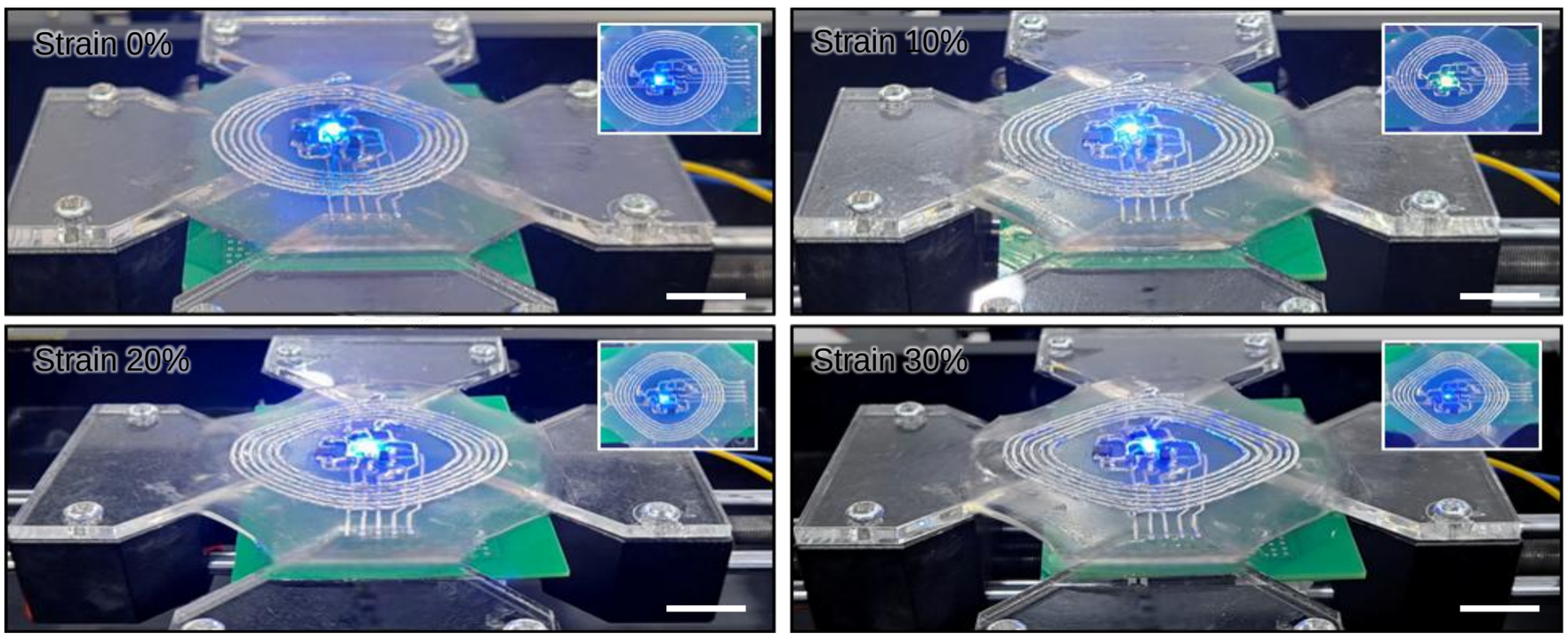
Supplementary Fig. 19. SEM characterization of Pt-LMP and AgNW composite electrodes. **a,** SEM image of the Pt-LMP composite electrodes. **b,** SEM image of the AgNW composite electrodes.



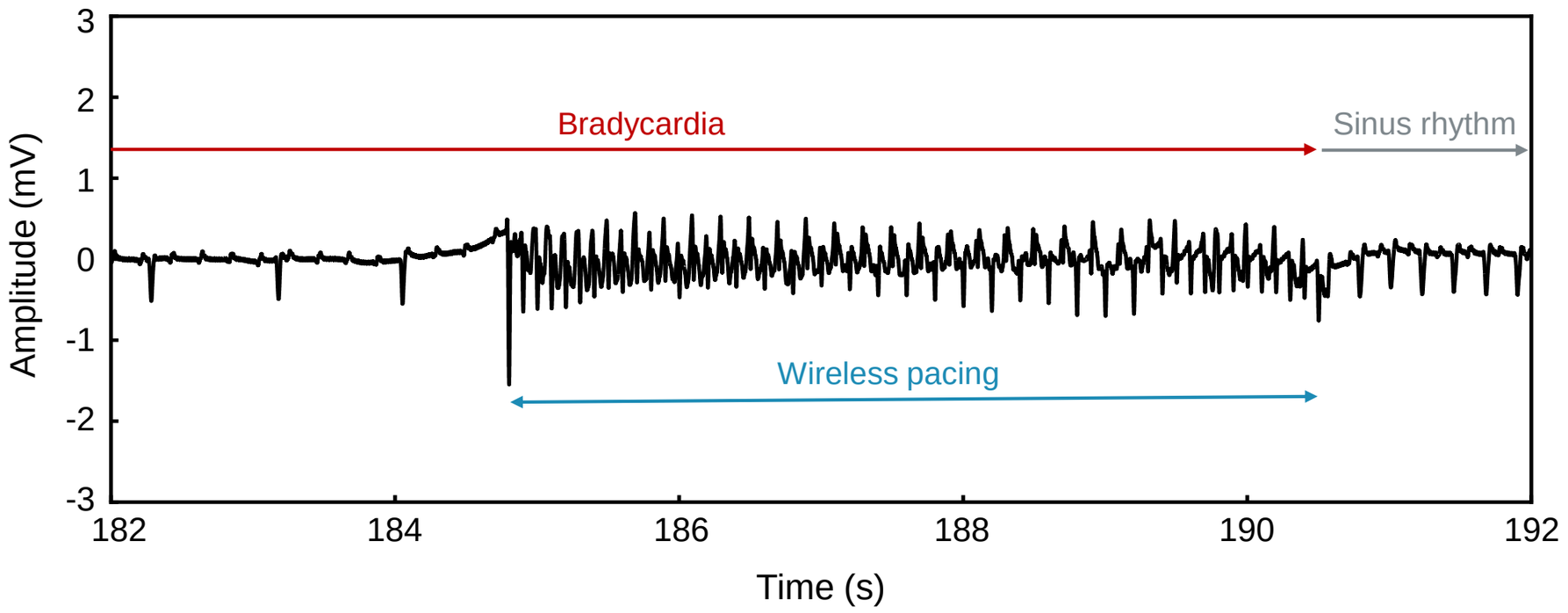
Supplementary Fig. 20. Electrochemical stability of AgNW composite electrodes after repeated stretching. a, Electrochemical impedance spectra. **b,** Cyclic voltammograms. **c,** Biphasic-pulse current responses measured before stretching and after 10, 100 stretching cycles.



Supplementary Fig. 21. Electrochemical stability of Pt-LMP electrodes after repeated stretching. a, Electrochemical impedance spectra. **b,** Cyclic voltammograms. **c,** Biphasic-pulse current responses measured before stretching and after 10, 100 stretching cycles.



Supplementary Fig. 22. Strain-resilient wireless powering of the stretchable circuit module under biaxial strain. Photographs showing sustained wireless powering, indicated by LED illumination, at 0%, 10%, 20% and 30% biaxial strain. Scale bar is 10 mm.



Supplementary Fig. 23. Representative surface ECG during bradycardia and wireless pacing. Representative surface ECG recording showing bradycardia, wireless pacing, and subsequent spontaneous sinus rhythm in a rat model.